Title
Low-Temperature Characterization of a Nonaqueous Liquid Electrolyte for Lithium Batteries

Journal
Journal of The Electrochemical Society, 171(3)

ISSN
0013-4651

Authors
Hickson, Darby T
Im, Julia
Halat, David M
et al.

Publication Date
2024-03-31

DOI
10.1149/1945-7111/ad2d91

Peer reviewed

Low Temperature Characterization of a Nonaqueous Liquid Electrolyte for Lithium Batteries

Darby Hickson, Julia Im, David M. Halat, Aakash Karvat, Jeffrey A. Reimer, Nitash Balsara
[1]*Materials Sciences Division and Joint Center for Energy Storage Research (JCESR), Lawrence Berkeley National Laboratory, Berkeley, California 94720, United States*
[2]*Department of Chemical and Biomolecular Engineering, University of California, Berkeley, Berkeley, California 94720, United States*

ABSTRACT

Rechargeable batteries exhibit poor performance at low temperatures due to sluggish ion transport through electrolytes. Ion transport is governed by three transport parameters – conductivity, diffusion coefficient, and the cation transference number with respect to the solvent velocity – and the thermodynamic factor. Understanding how these parameters change with temperature is necessary for designing improved electrolytes. In this work, we combine electrochemical techniques with electrophoretic NMR to determine the temperature dependence of these parameters for a liquid electrolyte, LiTFSI salt dissolved in tetraglyme between -20 and 45°C. At colder temperatures, all species in the electrolyte tend to move more slowly due to increasing viscosity, which translates to a monotonic decrease in conductivity and diffusion coefficient with decreasing temperature. Surprisingly, we find that the field-induced velocity of solvent molecules at a particular salt concentration is a nonmonotonic function of temperature. The cation transference number with respect to the solvent velocity thus exhibits a complex dependence on temperature and salt concentration. The measured thermodynamic and transport properties are used to predict concentration gradients that will form in a lithium-lithium symmetric cell under a constant applied potential as a function of temperature using concentrated solution theory. The calculated steady current at -20°C is lower than that at 45°C by factors ranging from 130 to 202.

INTRODUCTION

Lithium ion batteries suffer from worsened performance when operated at low ambient temperatures, which is a major hindrance to the adoption of electric vehicles (EVs) in colder climates.[1–3] Slow transport within a battery causes decreased range and power for EVs in the winter and charging at cold temperatures increases the likelihood of plating and cell failure.[4] Previous studies have identified many issues with operation at low temperature, including increased charge transfer resistance,[5–7] slow desolvation,[8] increased resistance through the solid electrolyte interphase (SEI),[9] and slow transport through porous electrodes.[10] Sluggish transport through the bulk electrolyte at low temperatures is one of the central reasons why battery performance suffers.[11] A transport property that is relatively easy to measure is ionic conductivity, and the temperature dependence of this property has been reported in several prior studies.[12–14] Current lithium ion battery electrolytes comprise mixtures of solvents such as ethylene carbonate (EC), a high dielectric constant solvent with high viscosity, and dimethyl carbonate (DMC), a low dielectric constant solvent with low viscosity. Reduced conductivity at low temperatures has been correlated to increases in electrolyte viscosity for EC/DMC and other

common carbonate based electrolytes.[12,13,15] Reducing the amount of EC has been investigated as an approach to lower the solvent viscosity and improve transport properties.[16–18] However, "EC-lean" electrolytes suffer from reduced conductivity and unstable electrode/electrolyte interfaces.[2,15,19] Generally, changing the solvent composition impacts the overall dielectric constant of the solvent and ion agglomeration,[15] which can impact the overall conductivity.[20–22] Engineering next generation electrolytes that will perform better over a wider temperature range is complex and must balance many material properties. Added complications arise due to the fact that ion transport in electrolytes depends on three additional properties that are seldom reported – salt diffusion coefficient, transference number, and the thermodynamic factor. These properties are much more difficult to measure and, not surprisingly, knowledge of their temperature dependence is limited.

The cation transference number, t_{+}^{0}, quantifies the fraction of the current carried by the cation with respect to the solvent velocity in an electrolyte of uniform concentration. Determining t_{+}^{0} based exclusively on electrochemical methods is complex and requires combining data from multiple experiments. Even studies at ambient temperatures have produced varying transference numbers for carbonate-based electrolytes, with each study utilizing a unique set of experiments with different levels of precision.[14,23–25] Comparison between transference numbers measured at ambient temperature has been reported elsewhere.[14,23] In the limited literature reporting transference numbers at multiple temperatures, conflicting trends have been reported. For a conventional, carbonate-based electrolyte, Ringsby et al. found that transference numbers were constant between 25 and -30°C using MD simulations.[15] This contrasted with experimental measurements of t_{+}^{0} obtained for the same electrolyte by Landesfeind and Gasteiger, who found that t_{+}^{0} decreased with decreasing temperature.[26] While there is no question that conductivity decreases with decreasing temperature, it is not clear if the same holds true for cation transference.

The experimental data described in the preceding paragraph are based on the quantification of cation transference based on electrochemical methods alone. In this approach, four independent experiments are used to determine the four relevant properties: conductivity, κ, salt diffusion coefficient, D, transference number, t_{+}^{0}, and a thermodynamic factor, T_f. The intrinsic coupling between t_{+}^{0} and T_f in the measured quantities compounds error and reduces measurement certainty.

In this work, we have characterized a simple liquid electrolyte, lithium bis(trifluoromethanesulfonyl)imide (LiTFSI) salt dissolved in tetraethylene glycol dimethyl ether (tetraglyme). We use electrophoretic NMR (eNMR) to determine t_{+}^{0} directly by measuring the electric-field-induced cation, anion, and solvent velocities.[27–29] In addition, we also conduct the four electrochemical experiments indicated in the preceding paragraph. Combining these five experiments significantly reduces measurement uncertainty in t_{+}^{0} and T_f. The electrochemical experiments were conducted over a wide temperature window from -20 to 45°C. Due to instrument limitations, the eNMR experiments could only be conducted from 15 to 45°C. In spite of this limitation, our measurements enable a comprehensive understanding of the many factors that underpin slow ion transport rates at low temperatures in LiTFSI/tetraglyme mixtures. The four parameters, κ, D, $\rho_{+,-}$, and T_f, are necessary for predicting the response of our electrolyte to an applied current. We use our measurements of these parameters to predict the steady-state salt

concentration profiles and current-potential relationships as a function of temperature in LiTFSI/tetraglyme mixtures.

EXPERIMENTAL

Electrolyte Preparation

Lithium bis(trifluoromethanesulfonyl) imide (LiTFSI) salt and tetraethylene glycol dimethyl ether (tetraglyme) were both acquired from Sigma-Aldrich and dried in a glovebox antechamber under active vacuum for three days at 60°C and 100°C. Electrolytes were prepared in an argon glovebox, where oxygen and water levels were kept below 1 ppm and stirred overnight at 25°C. The concentrations of electrolytes used in this study are listed in Table S1. The unit of concentration r corresponds to the ratio of lithium cations in LiTFSI to ether oxygens in tetraglyme, $r = ([Li^+]/[O])$.

Material Characterization

Density of each electrolyte was determined using an Anton Paar DMA 4101 density meter for each salt concentration between 10 and 100°C. Density (ρ¿ data is fully reported in Table S2. Viscosity (η) data was collected using an electro magnetically spinning viscometer (Kyoto Electronics). Density data was used to calculate molarity of electrolytes at each temperature, which is reported in Table S3. Viscosity measurements were obtained for each salt concentration and temperature from 0°C and 100°C and are presented in Figure 2b. The full set of viscosity data is listed in Table S4.

Conductivity

Coin cells were assembled using CR2032 coin cell parts (MTI Corp.) with five layers of Celgard 2500 separators soaked in electrolyte. At least three cells were made for each concentration, and cells were cycled in an environmental chamber (JEIO Tech) at a given temperature setpoint (45, 30, 15, 0, -20°C). Temperatures within the environmental chamber were corroborated using a thermocouple. Ac impedance spectroscopy measurements were obtained using a Biologic VMP300 potentiostat, using a frequency range of 1 MHz to 100 mHz with a sinus amplitude of 5 mV. Series resistance values, R_s, were obtained from the impedance spectra and can be related to the conductivity of an electrolyte via equation 1.[30]

$$\kappa = \frac{\tau}{\varphi_c}\frac{l}{R_s A}, \tag{1}$$

τ is the separator tortuosity, φ_c is the volume fraction of the conducting phase, l is the thickness of the separator, and A is the surface area of the electrodes. For Celgard 2500, φ_c is the porosity, 0.55. The tortuosity of the Celgard was previously determined and is 2.93.[31]

Current Fraction and Restricted Diffusion

Lithium-LiTFSI/tetraglyme-lithium symmetric cells were assembled in CR2032 coin cell parts (MTI Corp) using five, ten, or fifteen layers of electrolyte soaked Celgard 2500 separators. Separators were sandwiched between lithium chips (MTI Corp), 14 mm in diameter and 600 um thick. A minimum of three cells were made for each concentration and thickness. Cells were

cycled in an environmental chamber (JEIO Tech) to maintain a given temperature, which was corroborated using a thermocouple.

Cells were preconditioned to stabilize the SEI between the lithium metal electrodes and electrolyte. Alternating current densities of ±0.02 mA/cm^2 were applied for four hours using a potentiostat (Biologic, VMP300) until the interfacial resistance, R_i, was stable. Cells were allowed to rest for one hour in between polarizations. To measure the current fraction, $\rho_{+¿¿}$, also sometimes referred to as the ideal transference number or the Bruce-Vincent transference number,[32–34] cells were polarized at ΔV = 10 mV, -10 mV, 20 mV, and -20 mV for one hour. Multiple potentials were used to ensure the value of the current fraction was independent of applied potential. During polarization, the steady-state current, I_{ss}, was measured. Impedance measurements were taken before, during, and after polarization to determine $R_{i,0}$ and $R_{i,ss}$, the initial and steady-state interfacial resistances in the cell, respectively. I_Ω, the initial current in the cell, was determined using Ohm's law, assuming there are no concentration gradients within the cell at the start of polarization. The current fraction was calculated in accordance with equation 2.[32–34]

$$\rho_{+¿}=\frac{I_{ss}}{I_\Omega}\left(\frac{\Delta V-I_\Omega R_{i,0}}{\Delta V-I_{ss}R_{i,ss}}\right)_{,¿} \tag{2}$$

After polarization, the cell was allowed to relax and the open circuit potential, U, was monitored. Cells were allowed to relax for either 15 minutes, 1 hour, or 2.25 hours, for the five, ten, and fifteen Celgard cells, respectively, as relaxation times scale with length squared. The relaxation of the potential corresponds to the relaxation of the concentration gradient using the method of restricted diffusion.[35] U was fitted to an exponential, $U(t)=k_0+ae^{-bt}$, where k_0 is an offset voltage and a and b are determined from fitting. The diffusion coefficient through the separator, D_s, is related to the fit coefficient, b, via $D_s=\frac{l^2 b}{\pi^2}$. A minimum time cutoff is used such that $\alpha=\frac{D_s t}{l^2}>0.03$, which ensures the fit is independent of the steady-state concentration gradient formed during polarization.[36] The salt diffusion coefficient, D, was calculated by correcting D_s for the tortuosity of the separator, so that $D=\tau D_s$.

Concentration Cells

Previously, the thermodynamic factor was determined using large volume concentration cells made from glass U-cells.[31,37] This method was effective for room temperature measurements of the open circuit potential, as temperature did not need to be precisely controlled. For this work, pouch based concentration cells were adapted from Landesfeind et al.[26] A 1 cm wide, 10 cm long, and 25 um thick Celgard 2500 separator was placed in a pouch cell (5 cm wide, 13 cm long). The long separator ensures that complete mixing of the electrolyte via mutual diffusion will not occur during the measurement period. The separator was placed on top of lithium foil electrodes (MTI Corp.), which were affixed to nickel tabs using sealing tape. One side of the separator was wet with a reference electrolyte, r = 0.064, and the other side was wet with a test electrolyte. Care was taken to ensure the separator was fully wet without having excess electrolyte spill into the cell volume. The pouch cell was then sealed under argon.

The pouch cells were then moved to an environmental chamber (JEIO tech) and placed between metal blocks to ensure temperature equilibration during the measurement, which was

corroborated using a thermocouple. The open circuit potential for each concentration cell, U, was monitored at each temperature setpoint for 10 minutes and then the average value was taken. At least two pouch cells were made for each concentration.

Electrophoretic NMR (eNMR)

Details of eNMR experiments have been previously reported.[38,39] Instrumentation was based on the work done by Fang *et al*.[38] (P & L Scientific Instrument Service). Samples were prepared by filling a dried eNMR cell with electrolyte under an inert argon atmosphere. A convection-compensated double stimulated-echo (DSTE) PFG-NMR pulse program was used, with electric field pulses of opposite polarity applied.[40–42] Applied voltages ranged between 10 and 160 50 V, and all velocities were normalized to 1 V/mm. The electric field was applied for a constant drift time, Δ, of 100 ms. The electric field was allowed to equilibrate between electric field pulses using recycle delays of 60 12075 seconds. The electric field was calibrated at 25°C using a 10 mM solution of tetramethylammonium bromide (TMABr) dissolved in D_2O (P & L Scientific, Stockholm, SE). eNMR phase shifts were manually analyzed by calculating phase shifts as previously described.[38] ^{7}Li, ^{19}F, and ^{1}H NMR measurements were used to determine cation, anion, and solvent velocities, respectively; experiments were performed at a field strength of 9.4 T using a 400 MHz Bruker NEO spectrometer and a Bruker 5 mm water-cooled double resonance broadband diffusion (diffBB) probe, which was equipped with z-axis gradient capabilities (maximum gradient strength of 17 T m^{-1}) and variable-temperature control. Experiments were conducted at 45, 30, and 15 °C, ± 1 °C. The temperature range for measuring velocities from eNMR was limited to a maximum temperature of 15°C as the species' velocities at 15°C this temperature were close to the lower limit of instrument resolution instrumental measurement limits.

RESULTS AND DISCUSSION

In Figure 1a, we plot conductivity, κ, shown as a function of both r and molality, m. Conductivity shows a nonmonotonic dependence on salt concentration at all temperatures, increasing in the low concentration regime due to an increase in charge carriers and decreasing in the high concentration regime due to viscosity effects. At lower temperatures, conductivity markedly decreases: at -20°C, the electrolyte retains less than 12% of the 45°C conductivity at all salt concentrations. The conductivity decrease that occurs as temperature decreases has been well documented in literature.[2,15] A third order polynomial was fit through each data set in Figure 1a in order to determine the conductivity peak at a given temperature. The salt concentration where the conductivity maximum occurs, r_{max}, is plotted in Figure 1b. κ_{max}, the value at which the conductivity peaks, is also shown. Both r_{max} and κ_{max} decrease as temperature decreases. The fact that κ_{max} decreases by a factor of 17 is not very surprising. What is more surprising is the reduction of r_{max} by a factor of two. The onset of frictional effects occurs at significantly lower concentrations when temperature is reduced. Consequently, decreasing temperature has a more deleterious effect on conductivity in concentrated electrolytes; compare the spread of the data in Figure 1a for low and high salt concentrations.

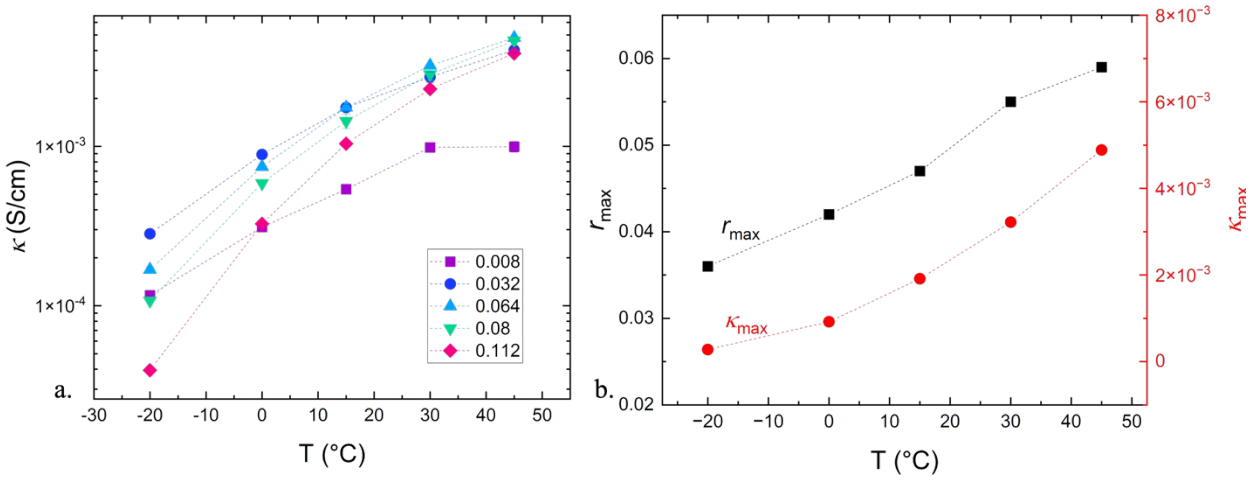

Figure *1*a. Conductivity data as a function of salt concentration and temperature, obtained using ac impedance spectroscopy. b.) Concentration at which conductivity peaks, r_{max}, plotted as a function of temperature. r_{max} was determined by fitting a third order polynomial to the measured conductivity data and determining the maximum. The corresponding conductivity at a given temperature, κ_{max}, is also plotted on the right y axis.

In Figure 2a, the molar conductivity (conductivity divided by salt concentration in mol/cm^3), Λ, is shown as a function of temperature (from -20 to 45°C). At the highest salt concentration, r = 0.112, Λ decreases by a factor of about 100, whereas at r = 0.008, the conductivity only decreases by a factor of about 10 over the same temperature range. In Figure 2b, we show the dependence of the viscosity, η, of LiTFSI/tetraglyme on salt concentration and temperature (from 0 to 100°C). η decreases by about a factor of 42 at r = 0.112 and by a factor of 7 at r = 0.008 over the measured range of temperatures. From this data, we can also see that the viscosity of the most concentrated electrolyte also changes much more rapidly with temperature than the dilute electrolyte.

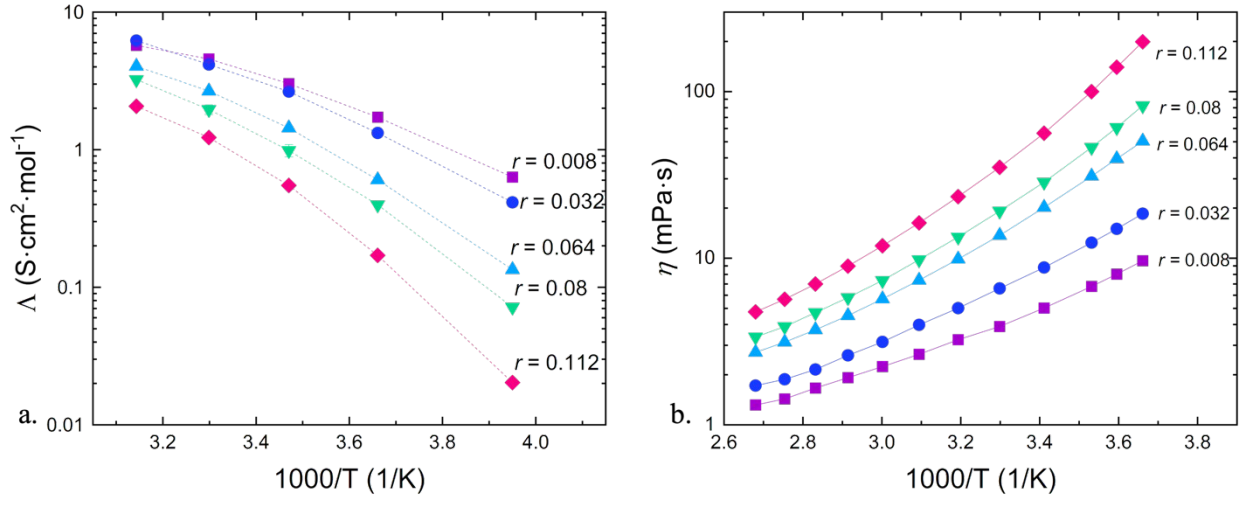

Figure 2. a) Molar conductivity is plotted as a function of inverse temperature. b) Viscosity data for corresponding salt concentrations is plotted as a function of inverse temperature. Figure inset corresponds to values of *r*.

The inverse relationship between conductivity and viscosity in liquid electrolytes is well established.[12,43,44] In the limit of infinite dilution, Walden observed that the product of the viscosity of pure water and molar conductance was independent of temperature, also referred to as the Walden product or Walden rule.[45,46] To examine this relationship in our system, we plot the product $\kappa\eta$ as a function of temperature in Figure 3. This product is a weak function of temperature at all salt concentrations, but this dependence becomes slightly stronger at higher salt concentrations. This indicates that the change in conductivity with temperature of LiTFSI/tetraglyme arises mainly due to changes in viscosity. Deviations from the Walden rule at higher concentrations are usually attributed to ion association.[47,48]

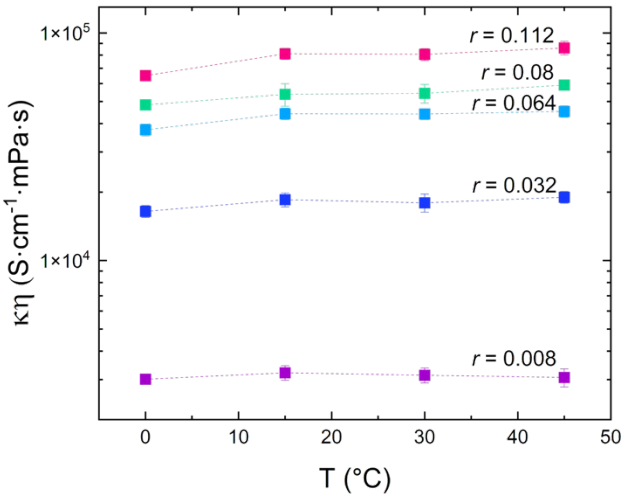

Figure *3*. The product of conductivity multiplied by viscosity is shown as a function of temperature for all salt concentrations.

The decrease in conductivity with decreasing temperature is well established in the literature. However, there are relatively few studies of the effect of temperature on other transport parameters. In Figure 4a, we show the dependence of current fraction, $\rho_{+¿¿}$, on salt concentration and temperature. Across all salt concentrations, $\rho_{+¿¿}$ decreases as temperature decreases. While κ is a more sensitive function of temperature at high salt concentrations, $\rho_{+¿¿}$ depends more strongly on temperature at low salt concentrations. In Figure 4b, we plot the product of $\kappa\,\rho_{+¿¿}$ as a function of temperature. In the limit of a small, applied dc potential, this product is proportional to the current that would be obtained in a given electrolyte. The data obtained from different values of r seem to collapse when plotted in this format (see Figure 4b). This is a manifestation of the compensating dependencies of κ and $\rho_{+¿¿}$ on salt concentration mentioned above. In the concentration range, $0.064 < r < 0.112$, $\kappa\,\rho_{+¿¿}$ decreases by a factor of 200 ± 16 over our temperature window. This factor reduces systematically with decreasing concentration: at $r = 0.032$, this factor is 131, while at $r = 0.008$, this factor is 43.

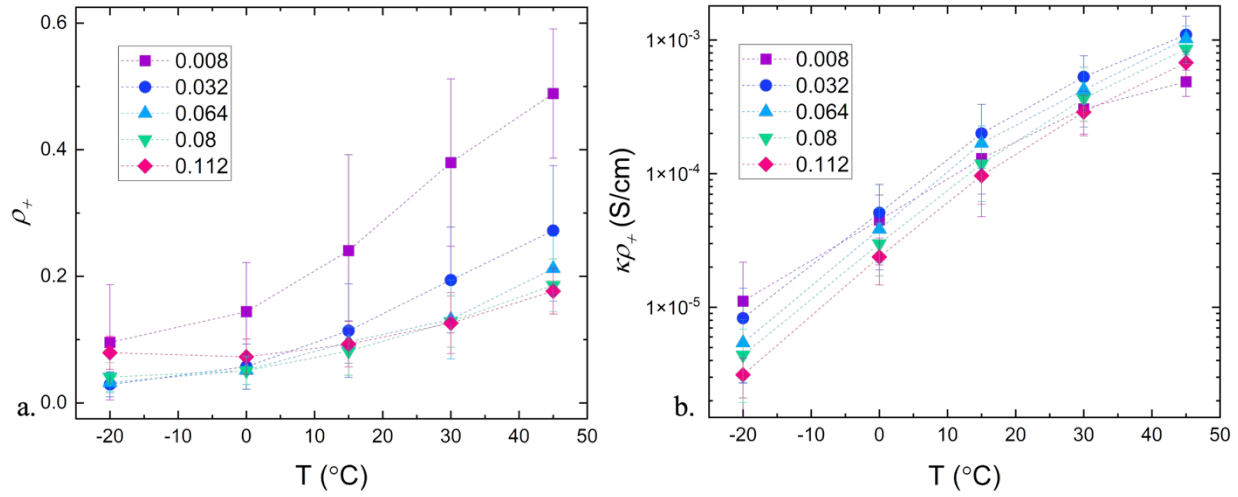

Figure *4*. a) Current fraction and b) effective conductivity, both plotted as a function of temperature. Figure insets corresponds to values of *r*.

The diffusion coefficient, *D*, measured using the restricted diffusion method,[35] is shown in Figure 5**.** At a given salt concentration, *D* is a weaker function of temperature when compared to κ. At $r = 0.008$, *D* decreases by a factor of 8 in our temperature window. This is somewhat lower than the decrease by a factor of 14 in κ. However, at $r = 0.112$, *D* only decreases by a factor of 4 while κ decreases by a factor of 100. Generally speaking, *D* deceases with increasing salt concentration. The surprising result in Figure 5 is *D* at -20°C is virtually independent of salt concentration (within experimental error). It is clear that *D* is not as strongly affected by solution viscosity as κ. The nonintuitive results in Figure 5 reflect the fact that *D* is affected by both thermodynamic and frictional contributions. We will attempt to separate these contributions in the discussion below.

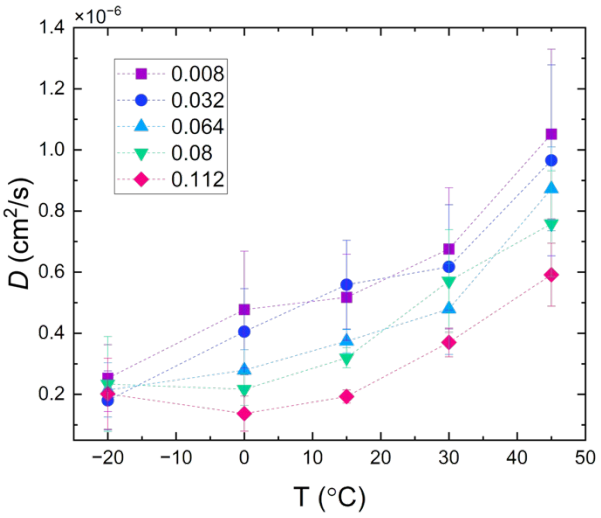

Figure *5*. Diffusion coefficients obtained using restricted diffusion, plotted as a function of temperature. Figure inset corresponds to values of *r*.

Transference numbers, $t_{+¿^0¿}$, in the temperature range of 15 to 45°C were determined using electrophoretic NMR. The species' velocities were determined under an applied potential of 1 V/mm; $v_{+¿¿}$ is the cation velocity, v_0 is the solvent velocity, and $v_{-¿¿}$ is the anion velocity. $t_{+¿^0¿}$ is given in equation 4.[49]

$$t_{+¿^0}=\frac{v_{+¿-v_0}}{v_{+¿-v_{-¿¿}}}¿¿ \tag{4}$$

Measured values for $v_{+¿¿}$, v_0, and $v_{-¿¿}$ using the laboratory reference frame are shown in Figure S2. Velocities of species in the direction of the negative electrode are defined as positive. For all electrolytes, $v_{+¿¿}$ and v_0 are positive while $v_{-¿¿}$ is negative. In general, the magnitude of all species' velocities decreases with decreasing temperature. The only exception to this is the solvent velocity for r = 0.08, which is a nonmonotonic function of temperature. The experimentally determined dependence of $t_{+¿^0¿}$ on r and temperature is shown in Figure 6. In the most dilute electrolyte, r = 0.008, $t_{+¿^0¿}$ is nearly independent of temperature. In the electrolyte with r = 0.032, $t_{+¿^0¿}$ decreases slightly with increasing temperature. More complex, nonmonotonic dependencies are seen in more concentrated electrolytes. The complex dependence of $t_{+¿^0¿}$ on temperature arises mainly due to the complex dependence of v_0 on salt concentration and temperature. The magnitude of $v_{+¿¿}$ relative to the sum of ion velocities, $v_{+¿+v_{-¿¿}¿}$, is not a strong function of temperature or salt concentration and varies between ~0.3 and 0.42 (see Figure S3). The lowest value of the $t_{+¿^0¿}$, -0.17, is obtained at r = 0.08 and T = 30°C. Under these conditions, the field-induced solvent velocity is larger than that of the cation.

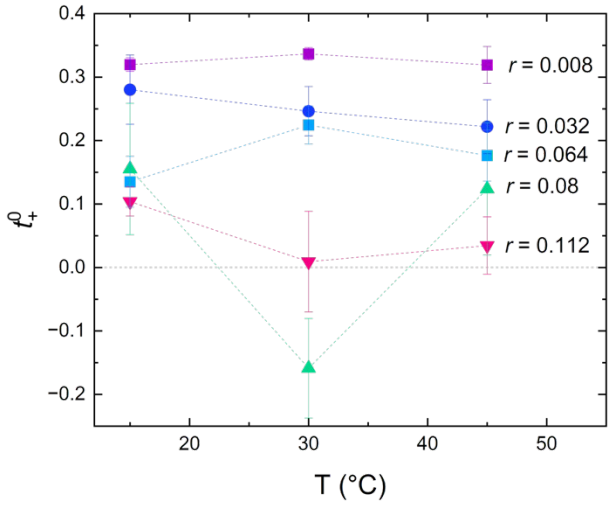

Figure 6. Cation transference number with respect to the solvent velocity, determined using electrophoretic NMR, plotted as a function of temperature.

The open circuit potential measured in a concentration cell, U❑❑, is plotted in Figure 7 as a function of ln(m) and temperature. The reference solution concentration was r = 0.064. At this concentration, the measured values of U, which are near zero, reflect errors in our measurements. U depends mostly on salt concentration and is a weak function of temperature. U is a more sensitive function of salt concentration at low temperatures. Our approach requires

evaluation of dU/dln(m), which we ~~get~~ obtain using a finite difference approach, described previously.[31]

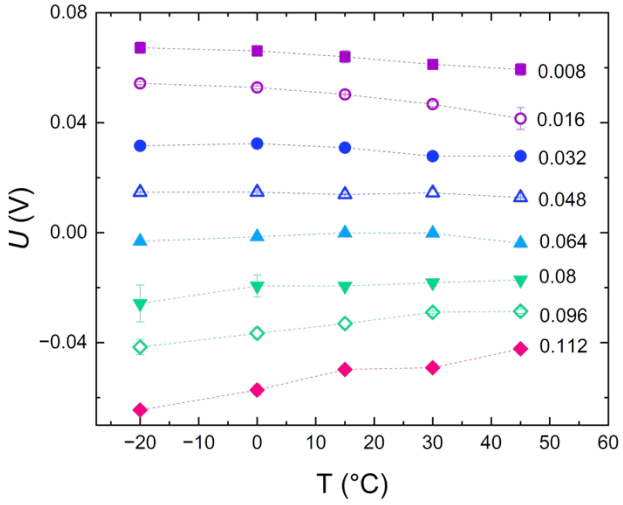

Figure 7. Open circuit potential determined in concentration cells, U ❑, plotted as a function of temperature. Line labels refer to r for the test concentration. The reference concentration was r = 0.064.

The thermodynamic factor, T_f, is given by:

$$T_f = 1 + d\ln\frac{y_{\pm ¿}}{d\ln m} = \frac{F}{2RT ¿¿}¿ \qquad (5)$$

where $y_{\pm ¿¿}$ is the mean molal salt activity coefficient. Using only $t_{+¿^0¿}$ values given in Figure 6 and dU/dln(m) values determined from Figure 7, we obtain the dependence of T_f on concentration and temperature. Generally speaking, T_f increases with increasing salt concentration. A slight decrease of T_f is observed when salt concentration is increased from r = 0.064 to 0.08 at 30°C. This is mainly due to the nonmonotonic dependence of $t_{+¿^0¿}$ on temperature at $r-$ = 0.08. The complex dependence of $t_{+¿^0¿}$~~t+0~~ on temperature arises mainly due to the complex dependence of v_0~~v0~~ on temperature at this salt concentration.

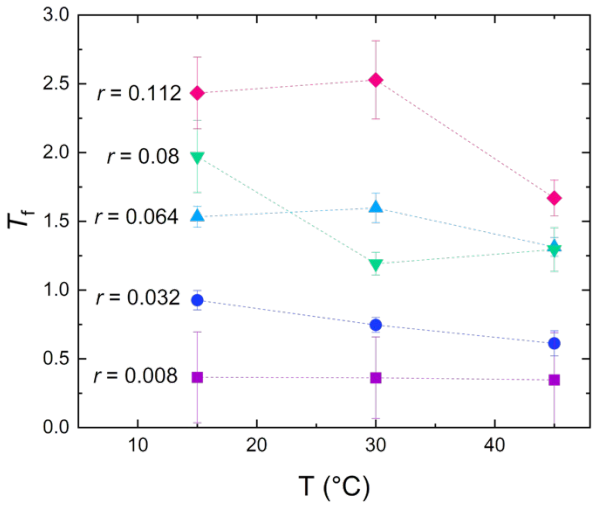

Figure 8. Thermodynamic factor, T_f, determined using transference numbers from eNMR and data from concentration cell experiments.

The salt diffusion coefficient, D, is dependent on both frictional and thermodynamic effects, which results in a complex dependence on both salt concentration and temperature (Figure 5). One expects D to decrease with increasing viscosity, η, and therefore is instructive to examine the product $D\eta$. This is analogous to the product $\kappa\eta$, plotted in Figure 3. The dependence of $D\eta$ on salt concentration and temperature is shown in Figure 9a. It is evident that the complex dependence of D on salt concentration and temperature is not just due to changes in viscosity. The product $D\eta$ is a stronger function of temperature in more concentrated electrolytes. The complexity in Figure 9a reflects the fact that D depends on both thermodynamics and frictional effects. One can define a Stefan-Maxwell diffusion coefficient, $\mathcal{D}$, which quantifies diffusion based on a thermodynamic driving force,[50]

$$D = \mathcal{D}\frac{c_0}{c_T T_f}, \tag{6}$$

where c_0 is the solvent concentration and c_T is the total concentration of the salt and solvent, $c_T = c_0 + c$. The dependence of $D\eta$~~script Deta~~ on salt concentration and temperature is shown in Figure 9b. At the lowest concentration, r = 0.008, the differences between $D\eta$ and $\mathcal{D}\eta$ are minor. The difference between $D\eta$ and $\mathcal{D}\eta$ increases with increasing r~~r~~. This implies that the corrections to D due to thermodynamic effects become more important as r increases. To a good approximation, the product $\mathcal{D}\eta$ is equal to $(7\pm3)\times10^{-6}$ cm^{2}mPa, irrespective of temperature and salt concentration. The product $\mathcal{D}\eta$~~script D eta~~, is noteworthy as it is more-or-less independent of both temperature and salt concentration. Measurement of T_f ~~Tf~~ enables the separation of these frictional and thermodynamic interactions.

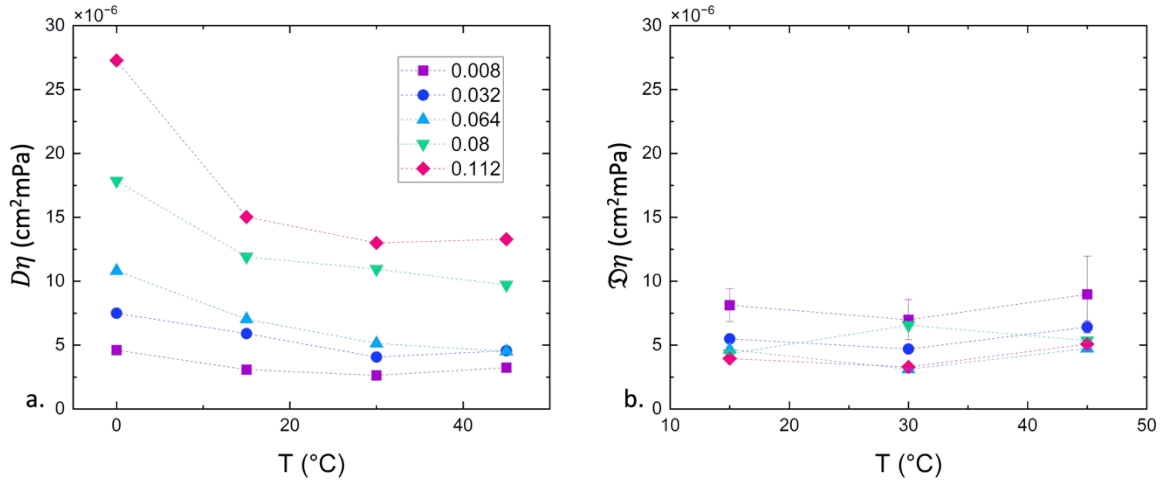

Figure 9. The product of diffusion coefficients and viscosity for, a. the salt diffusion coefficient and b. Stefan-Maxwell diffusion coefficients, plotted as a function of both salt concentration and temperature.

In the discussion above, we present complete characterization of LiTFSI/tetraglyme as a function of concentration and temperature. This enables predictions of concentration gradients that arise in the electrolyte due to the passage of current.[51–53] Large concentration gradients result in large concentration overpotentials which decrease the rate at which electrochemical reactions occur at the electrodes.[54–59] We calculate salt concentration and potential gradients as a function of applied current using concentrated solution theory in a symmetric lithium-LiTFSI/tetraglyme-lithium cell. The concentration profile is determined using equation 6,[51]

$$\int_{r(x=0)}^{r(x)} \kappa\left(\frac{dU}{dlnm}\right) \text{¿¿¿} \tag{6}$$

where i_{ss} is the steady-state applied current, L is the distance between electrodes, $z_{-\text{¿¿}}$ is the anion charge number, and $v_{-\text{¿¿}}$ is the number of anions the salt dissolves into. x/L refers to the dimensionless position across the electrolyte. $x/L = 0$ is the positive electrode where salt accumulates. $x/L = 1$ is the negative electrode where salt is depleted. The potential of the positive electrode relative to that of the negative is given by Φ_{ss} Equation 7,[51]

$$\Phi_{ss}(x=0) = -F\, z_{-\text{¿}} v_{-\text{¿}} \int_{r(x=L)}^{r(x=0)} \left(\frac{dU}{dlnm}\right) \text{¿¿¿} \text{¿} \tag{7}$$

In order to solve for $r(x=0)$ and Φ_{ss} $(x=0)$, we need expressions that quantify the dependence of κ, $dU/dlnm$, and $\rho_{+\text{¿¿}}$ on temperature and concentration. These expressions were obtained by fitting the experimental data presented above and the fits are listed in Table S5. These fits are used to determine the concentration dependence of the integrands in equations 6 and 7. To facilitate calculations, the integrands were also fit to continuous functions that are given in Table S6 and S7.

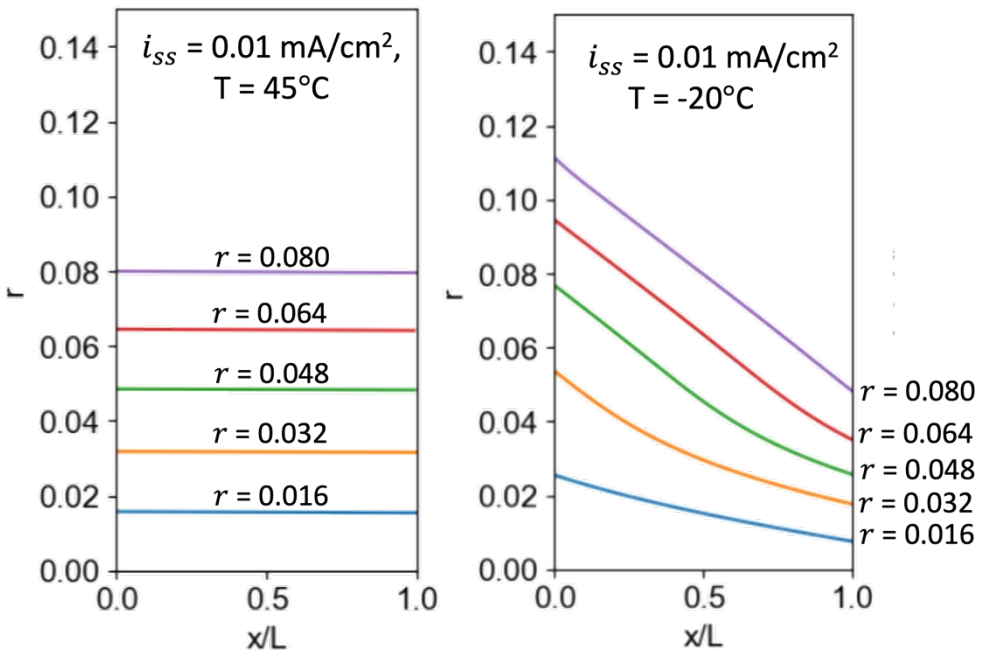

Figure 10. Results from modeled concentration gradients, based on measured electrochemical data. Predicted concentration gradients for multiple concentrations are shown for 45°C and -20°C for an applied steady state current density of 0.01 mA/cm².

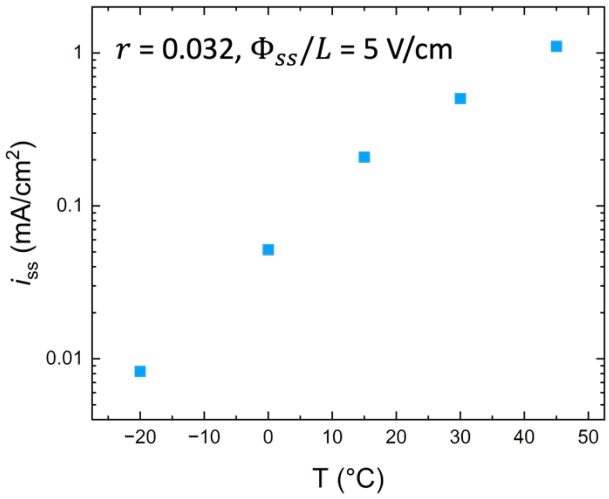

Figure 11. Results from modeled potential gradients, based on measured electrochemical data. For a given length normalized applied potential, here 5 V/cm, the resulting current at steady state is shown for an example salt concentration, r = 0.032.

In Figure 10, we show results for a fixed applied steady state, i_{ss} of 0.01 mA/cm.[2] The average concentration of the electrolyte, r_{avg}, was ~~changed~~ varied from 0.016 to 0.08. The results at 45°C are shown in Figure 10a. At this temperature, the magnitudes of the salt concentration gradients are negligible. The results at -20°C are shown in Figure 10b. Here we see substantial salt concentration gradients and the magnitude increases with increasing salt concentration. In the limit of infinite dilution wherein the electrolyte is thermodynamically ideal and transport parameters are independent of concentration, the salt concentration profile is linear.[50] It is thus

not surprising that the profile at r_{avg}~~r_avg~~ = 0.016 is approximately linear. Significantly, nonlinearity is seen when salt concentration is increased to r_{avg} = 0.032. Nonlinear contributions appear to decrease with increasing concentration and r_{avg}~~r~~ = 0.08, the concentration profile is, to a good approximation, linear. The salt concentration profiles depend on three concentration dependent parameters, κ, $dU/dlnm$, and $\rho_{+¿¿}$~~k, dU/dlnm, and rho+~~, and these parameters can combine in nontrivial ways to give surprising results.

In Figure 11, we show results for a fixed applied length-normalized potential, Φ_{ss}/L~~phiss/L~~, of 5 V/cm in an electrolyte with r_{avg}~~r~~ = 0.032. This polarization results in a steady- state current, i_{ss}~~i_ss~~, of 1.1 mA/cm^2 at 45˚C. The current obtained drops precipitously with decreasing temperature and at -20˚C, we obtain i_{ss}~~iss~~ of 0.008 mA/cm^2. In other words, the current obtained decreases by a factor of 130 when temperature is changed from 45 to -20˚C. We repeated these calculations for r_{avg}~~r-avg~~ = 0.064 and 0.08. The factors by which current decreased over the same temperature range were 202 and 190, respectively. If the r_{avg}~~r~~ = 0.08 electrolyte was used in a rechargeable battery that was charged in one hour at 45˚C, it would take 190 hours at -20˚C.

Comparison to Literature

While LiTFSI/tetraglyme electrolytes have been studied previously,[31,60–62] we are not aware of prior studies that have characterized the LiTFSI/tetraglyme electrolyte over a wide temperature range. However, mixtures of $LiPF_6$ and carbonate solvents (e.g., ethylene carbonate, EC, ethyl methyl carbonate, EMC, and dimethyl carbonate, DMC) have been studied over a wide temperature range. We therefore compare our results with published data on these systems to examine which general trends hold true for liquid electrolytes. Ions move slower at lower temperatures. This impacts ionic conductivity, which reflects field-induced motion of cations and anions, and the salt diffusion coefficient, which reflects the rate at which concentration gradients relax. Not surprisingly, a decrease in both conductivity (κ) and diffusion coefficients (D) with decreasing temperature has been found in all liquid electrolytes,[13,14,63] including LiTFSI/tetraglyme (Figures 1a and 5). However, D is affected by both frictional and thermodynamic effects, and we present data on Stefan-Maxwell diffusion coefficients, D, that is affected by frictional effects only (Figure 9). None of the previous experimental studies of temperature-dependent properties of liquid electrolytes have reported D.

There are conflicting reports on the effect of temperature on the cation transference number, $t_{+¿^0¿}$. Landesfeind and Gasteiger found $t_{+¿^0¿}$ to be a strong function of temperature in a 1 mol/L $LiPF_6$ in EC/EMC, decreasing from 0.35 at 25˚C to -0.5 at -20˚C.[26] Lundgren et al. also found that transference numbers decreased with decreasing temperature, but this depended on salt concentration. They found $t_{+¿^0¿}$ decreased from 0.27 at 40˚C to 0.16 at 10˚C for 0.5 mol/L $LiPF_6$ in EC/DEC, but it only decreased from 0.08 to 0.05 at 1.5 mol/L.[64] In contrast, simulations of Ringsby et al. suggest that $t_{+¿^0¿}$ is approximately 0.3 in 1 mol/L $LiPF_6$ in EC/EMC electrolytes between -20 and 30˚C.[15] Temperature-independent transference numbers were also obtained using the Advanced Electrolyte Model, which predicted $t_{+¿^0¿}$ near 0.5 at both 60 and -30˚C in the same electrolyte.[14,65] The reason for the discrepancy between theory and experiment in carbonate electrolytes remains unresolved. The results in carbonate electrolytes are very different from the $t_{+¿^0¿}$ data in tetraglyme (Figure 6). Much of the complexity seen in Figure 6 arises due to the field induced motion of solvent molecules (v_0, Figure S3).

The effect of temperature on the thermodynamic factor, T_f, is subtle relative to the effect of concentration. This was reported by Landesfeind and Gasteiger in EC/DMC and EC/EMC. This is consistent with the tetraglyme data reported here (Figure 8). In the carbonate electrolytes, T_f decreases with decreasing temperature. The data from tetraglyme electrolytes reported here is more-or-less consistent with this observation.

Unlike κ and ~~script~~ D, t_{+}^{0} and T_f are affected by many factors that can change with temperature in unpredictable ways. For example, Ringsby et al. studied ion clustering in liquid electrolytes as a function of temperature using molecular dynamics simulations, and found that the concentration of free Li^+ ions was larger at -20°C compared to 30°C.[15] This was attributed to an increase in the solvent dielectric constant with decreasing temperature.[66] Since t_{+}^{0} reflects the average field-induced-velocity of the cations (including free cations and clustered cations), the concentration of Li^+ ions will affect t_{+}^{0}. In spite of this, Ringsby et al. obtained a value of t_{+}^{0} that was independent of temperature. Previous molecular dynamics studies have examined ion clustering and agglomeration at various salt concentrations for LiTFSI/tetraglyme electrolytes, which explains the complex dependence of t_{+}^{0} on salt concentration.[38,67]

CONCLUSIONS

In this work, we combined electrochemical measurements with electrophoretic NMR to determine transport and thermodynamic properties of a liquid electrolyte, LiTFSI salt dissolved in tetraglyme. We have studied this electrolyte from -20°C to 45°C to determine how conductivity, diffusion coefficient, the cation transference number, and the thermodynamic factor change with temperature. Both conductivity and concentration-based salt diffusion coefficient decrease with decreasing temperature, but the magnitude of this decrease strongly depends on concentration. The product of viscosity and conductivity is nearly independent of temperature but a strong function of concentration. The product of viscosity and the Stefan-Maxwell diffusion coefficient, which is based on a thermodynamic driving force, is nearly independent of both concentration and temperature. The cation transference number with respect to the solvent velocity, t_{+}^{0}, reflects field-induced velocities of ions and solvent molecules. While the velocities of the ions decrease monotonically with temperature, the solvent velocity exhibits a maximum at 30°C for one salt concentration (r = 0.08). t_{+}^{0} thus exhibits a complex dependence on concentration and temperature. In contrast, the thermodynamic factor is a weak function of temperature.

We have used concentrated solution theory and the transport and thermodynamic properties described in the preceding paragraph to predict concentration gradients that will form in a lithium-lithium symmetric cell under a constant applied potential as a function of temperature. The steady current obtained in these cells decrease as the magnitude of the concentration gradients increase. The steady current at -20°C is lower than that at 45°C by factors ~~range~~ ranging from 130 to 202. The power available in batteries with LiTFSI/tetraglyme electrolytes would be drastically lower at -20°C relative to 45°C due, primarily, to the temperature dependence of transport properties.

ACKNOWELDGEMENTS

This work was primarily supported by the Vehicle Technologies Office of the U.S. Department of Energy's Office of Energy Efficiency and Renewable Energy under the guidance of the Advanced Battery Cell Research Program (eXtreme fast charge Cell Evaluation of Lithium-ion batteries, XCEL). Initial work was supported by the Assistant Secretary for Energy Efficiency and Renewable Energy, Vehicle Technologies Office, of the U.S. Department of Energy under Contract DE-AC02-05CH11231, under the Low Temperature Electrolyte program. We thank Dr Hasan Celik and UC Berkeley's NMR facility in the College of Chemistry (CoC-NMR) for spectroscopic assistance. The NMR instrument used in this work was supported by the National Science Foundation under grant no. 2018784. D.M.H. gratefully acknowledges support as a Pines Magnetic Resonance Center Postdoctoral Fellow; J.I. also acknowledges support from the Pines Magnetic Resonance Center.

AUTHOR CONTRIBUTIONS

CONFLICTS OF INTEREST

There are no conflicts of interest to declare.

BIBLIOGRAPHY

(1) Zhang, J.; Zhang, J.; Liu, T.; Wu, H.; Tian, S.; Zhou, L.; Zhang, B.; Cui, G. Toward Low-Temperature Lithium Batteries: Advances and Prospects of Unconventional Electrolytes. *Adv. Energy Sustain. Res.* **2021**, *2* (10), 2100039. https://doi.org/10.1002/aesr.202100039.

(2) Hubble, D.; Brown, D. E.; Zhao, Y.; Fang, C.; Lau, J.; McCloskey, B. D.; Liu, G. Liquid Electrolyte Development for Low-Temperature Lithium-Ion Batteries. *Energy Environ. Sci.* **2022**, *15* (2), 550–578. https://doi.org/10.1039/D1EE01789F.

(3) Xu, K. Nonaqueous Liquid Electrolytes for Lithium-Based Rechargeable Batteries. *Chem. Rev.* **2004**, *104* (10), 4303–4418. https://doi.org/10.1021/cr030203g.

(4) Lin, H. -p.; Chua, D.; Salomon, M.; Shiao, H.-C.; Hendrickson, M.; Plichta, E.; Slane, S. Low-Temperature Behavior of Li-Ion Cells. *Electrochem. Solid-State Lett.* **2001**, *4* (6), A71. https://doi.org/10.1149/1.1368736.

(5) Jow, T. R.; Ding, M. S.; Xu, K.; Zhang, S. S.; Allen, J. L.; Amine, K.; Henriksen, G. L. Nonaqueous Electrolytes for Wide-Temperature-Range Operation of Li-Ion Cells. *J. Power Sources* **2003**, *119–121*, 343–348. https://doi.org/10.1016/S0378-7753(03)00153-8.

(6) Zhang, S. S.; Xu, K.; Jow, T. R. The Low Temperature Performance of Li-Ion Batteries. *J. Power Sources* **2003**, *115* (1), 137–140. https://doi.org/10.1016/S0378-7753(02)00618-3.

(7) Jow, R.; Zhang, S. S.; Xu, K.; Allen, J. Electrolytes for Low Temperature Operations of Li-Ion Batteries. *ECS Trans.* **2007**, *3* (27), 51–58. https://doi.org/10.1149/1.2793578.

(8) Li, Q.; Lu, D.; Zheng, J.; Jiao, S.; Luo, L.; Wang, C.-M.; Xu, K.; Zhang, J.-G.; Xu, W. Li^+-Desolvation Dictating Lithium-Ion Battery's Low-Temperature Performances. *ACS Appl. Mater. Interfaces* **2017**, *9* (49), 42761–42768. https://doi.org/10.1021/acsami.7b13887.

(9) Wang, C.; Appleby, A. J.; Little, F. E. Low-Temperature Characterization of Lithium-Ion Carbon Anodes via Microperturbation Measurement. *J. Electrochem. Soc.* **2002**, *149* (6), A754. https://doi.org/10.1149/1.1474427.

(10) Huang, C.-K.; Sakamoto, J. S.; Wolfenstine, J.; Surampudi, S. The Limits of Low-Temperature Performance of Li-Ion Cells. *J. Electrochem. Soc.* **2000**, *147* (8), 2893. https://doi.org/10.1149/1.1393622.

(11) Smart, M. C.; Ratnakumar, B. V.; Surampudi, S. Electrolytes for Low-Temperature Lithium Batteries Based on Ternary Mixtures of Aliphatic Carbonates. *J. Electrochem. Soc.* **1999**, *146* (2), 486–492. https://doi.org/10.1149/1.1391633.

(12) Logan, E. R.; Tonita, E. M.; Gering, K. L.; Li, J.; Ma, X.; Beaulieu, L. Y.; Dahn, J. R. A Study of the Physical Properties of Li-Ion Battery Electrolytes Containing Esters. *J. Electrochem. Soc.* **2018**, *165* (2), A21–A30. https://doi.org/10.1149/2.0271802jes.

(13) Ma, X.; Arumugam, R. S.; Ma, L.; Logan, E.; Tonita, E.; Xia, J.; Petibon, R.; Kohn, S.; Dahn, J. R. A Study of Three Ester Co-Solvents in Lithium-Ion Cells. *J. Electrochem. Soc.* **2017**, *164* (14), A3556–A3562. https://doi.org/10.1149/2.0411714jes.

(14) Valøen, L. O.; Reimers, J. N. Transport Properties of LiPF6-Based Li-Ion Battery Electrolytes. *J. Electrochem. Soc.*

(15) Ringsby, A. J.; Fong, K. D.; Self, J.; Bergstrom, H. K.; McCloskey, B. D.; Persson, K. A. Transport Phenomena in Low Temperature Lithium-Ion Battery Electrolytes. *J. Electrochem. Soc.* **2021**, *168* (8), 080501. https://doi.org/10.1149/1945-7111/ac1735.

(16) Ma, L.; Glazier, S. L.; Petibon, R.; Xia, J.; Peters, J. M.; Liu, Q.; Allen, J.; Doig, R. N. C.; Dahn, J. R. A Guide to Ethylene Carbonate-Free Electrolyte Making for Li-Ion Cells. *J. Electrochem. Soc.* **2017**, *164* (1), A5008–A5018. https://doi.org/10.1149/2.0191701jes.

(17) Lazar, M. L.; Lucht, B. L. Carbonate Free Electrolyte for Lithium Ion Batteries Containing γ-Butyrolactone and Methyl Butyrate. *J. Electrochem. Soc.* **2015**, *162* (6), A928–A934. https://doi.org/10.1149/2.0601506jes.

(18) Petibon, R.; Harlow, J.; Le, D. B.; Dahn, J. R. The Use of Ethyl Acetate and Methyl Propanoate in Combination with Vinylene Carbonate as Ethylene Carbonate-Free Solvent Blends for Electrolytes in Li-Ion Batteries. *Electrochimica Acta* **2015**, *154*, 227–234. https://doi.org/10.1016/j.electacta.2014.12.084.

(19) Ma, X.; Li, J.; Glazier, S. L.; Ma, L.; Gering, K. L.; Dahn, J. R. A Study of Highly Conductive Ester Co-Solvents in Li[Ni0.5Mn0.3Co0.2]O2/Graphite Pouch Cells. *Electrochimica Acta* **2018**, *270*, 215–223. https://doi.org/10.1016/j.electacta.2018.03.006.

(20) Krachkovskiy, S. A.; Bazak, J. D.; Fraser, S.; Halalay, I. C.; Goward, G. R. Determination of Mass Transfer Parameters and Ionic Association of $LiPF_6$: Organic Carbonates Solutions. *J. Electrochem. Soc.* **2017**, *164* (4), A912–A916. https://doi.org/10.1149/2.1531704jes.

(21) Ding, M. S.; Xu, K.; Zhang, S. S.; Amine, K.; Henriksen, G. L.; Jow, T. R. Change of Conductivity with Salt Content, Solvent Composition, and Temperature for Electrolytes of LiPF6 in Ethylene Carbonate-Ethyl Methyl Carbonate. *J. Electrochem. Soc.*

(22) France-Lanord, A.; Grossman, J. C. Correlations from Ion Pairing and the Nernst-Einstein Equation. *Phys. Rev. Lett.* **2019**, *122* (13), 136001. https://doi.org/10.1103/PhysRevLett.122.136001.

(23) Ehrl, A.; Landesfeind, J.; Wall, W. A.; Gasteiger, H. A. Determination of Transport Parameters in Liquid Binary Electrolytes: Part II. Transference Number. *J. Electrochem. Soc.* **2017**, *164* (12), A2716–A2731. https://doi.org/10.1149/2.1681712jes.

(24) Nyman, A.; Behm, M.; Lindbergh, G. Electrochemical Characterisation and Modelling of the Mass Transport Phenomena in LiPF6–EC–EMC Electrolyte. *Electrochimica Acta* **2008**, *53* (22), 6356–6365. https://doi.org/10.1016/j.electacta.2008.04.023.
(25) Hou, T.; Monroe, C. W. Composition-Dependent Thermodynamic and Mass-Transport Characterization of Lithium Hexafluorophosphate in Propylene Carbonate. *Electrochimica Acta* **2020**, *332*, 135085. https://doi.org/10.1016/j.electacta.2019.135085.
(26) Landesfeind, J.; Gasteiger, H. A. Temperature and Concentration Dependence of the Ionic Transport Properties of Lithium-Ion Battery Electrolytes. *J. Electrochem. Soc.* **2019**, *166* (14), A3079–A3097. https://doi.org/10.1149/2.0571912jes.
(27) Gouverneur, M.; Kopp, J.; Van Wüllen, L.; Schönhoff, M. Direct Determination of Ionic Transference Numbers in Ionic Liquids by Electrophoretic NMR. *Phys. Chem. Chem. Phys.* **2015**, *17* (45), 30680–30686. https://doi.org/10.1039/C5CP05753A.
(28) Holz, M. Electrophoretic NMR. *Chem. Soc. Rev.* **1994**, *23* (3), 165. https://doi.org/10.1039/cs9942300165.
(29) Walls, H. J. Anion and Cation Transference Numbers Determined by Electrophoretic NMR of Polymer Electrolytes Sum to Unity. *Electrochem. Solid-State Lett.* **1999**, *3* (7), 321. https://doi.org/10.1149/1.1391136.
(30) Shah, D. B.; Nguyen, H. Q.; Grundy, L. S.; Olson, K. R.; Mecham, S. J.; DeSimone, J. M.; Balsara, N. P. Difference between Approximate and Rigorously Measured Transference Numbers in Fluorinated Electrolytes. *Phys. Chem. Chem. Phys.* **2019**, *21* (15), 7857–7866. https://doi.org/10.1039/C9CP00216B.
(31) Hickson, D. T.; Halat, D. M.; Ho, A. S.; Reimer, J. A.; Balsara, N. P. Complete Characterization of a Lithium Battery Electrolyte Using a Combination of Electrophoretic NMR and Electrochemical Methods. *Phys. Chem. Chem. Phys.* **2022**, *24* (43), 26591–26599. https://doi.org/10.1039/D2CP02622H.
(32) Watanabe, M.; Nagano, S.; Sanui, K.; Ogata, N. Estimation of Li+ Transport Number in Polymer Electrolytes by the Combination of Complex Impedance and Potentiostatic Polarization Measurements.
(33) Evans, J.; Vincent, C. A.; Bruce, P. G. Electrochemical Measurement of Transference Numbers in Polymer Electrolytes. *Polymer* **1987**, *28* (13), 2324–2328. https://doi.org/10.1016/0032-3861(87)90394-6.
(34) Bruce, P. G.; Vincent, C. A. Steady State Current Flow in Solid Binary Electrolyte Cells. *J. Electroanal. Chem. Interfacial Electrochem.* **1987**, *225* (1–2), 1–17. https://doi.org/10.1016/0022-0728(87)80001-3.
(35) Newman, J.; Chapman, T. W. Restricted Diffusion in Binary Solutions. *AIChE J.* **1973**, *19* (2), 343–348. https://doi.org/10.1002/aic.690190220.
(36) Thompson, S. D.; Newman, J. Differential Diffusion Coefficients of Sodium Polysulfide Melts. *J. Electrochem. Soc.* **1989**, *136* (11), 3362–3369. https://doi.org/10.1149/1.2096451.
(37) Stewart, S.; Newman, J. Measuring the Salt Activity Coefficient in Lithium-Battery Electrolytes. *J. Electrochem. Soc.* **2008**, *155* (6), A458. https://doi.org/10.1149/1.2904526.
(38) Halat, D. M.; Fang, C.; Hickson, D.; Mistry, A.; Reimer, J. A.; Balsara, N. P.; Wang, R. Electric-Field-Induced Spatially Dynamic Heterogeneity of Solvent Motion and Cation Transference in Electrolytes. *Phys. Rev. Lett.* **2022**, *128* (19), 198002. https://doi.org/10.1103/PhysRevLett.128.198002.

(39) Chakraborty, S.; Halat, D. M.; Im, J.; Hickson, D. T.; Reimer, J. A.; Balsara, N. P. Lithium Transference in Electrolytes with Star-Shaped Multivalent Anions Measured by Electrophoretic NMR. *Phys. Chem. Chem. Phys.* **2023**, *25* (31), 21065–21073. https://doi.org/10.1039/D3CP00923H.

(40) Jerschow, A.; Müller, N. Convection Compensation in Gradient Enhanced Nuclear Magnetic Resonance Spectroscopy. *J. Magn. Reson.* **1998**, *132* (1), 13–18. https://doi.org/10.1006/jmre.1998.1400.

(41) He, Q.; Wei, Z. Convection Compensated Electrophoretic NMR. *J. Magn. Reson.* **2001**, *150* (2), 126–131. https://doi.org/10.1006/jmre.2001.2321.

(42) Pettersson, E.; Furó, I.; Stilbs, P. On Experimental Aspects of Electrophoretic NMR: Experimental Electrophoretic NMR. *Concepts Magn. Reson. Part A* **2004**, *22A* (2), 61–68. https://doi.org/10.1002/cmr.a.20012.

(43) Robinson, R. A.; Stokes, R. H. *Electrolyte Solutions*, 2nd rev. ed.; Dover Publications: Mineola, NY, 2002.

(44) Schreiner, C.; Zugmann, S.; Hartl, R.; Gores, H. J. Fractional Walden Rule for Ionic Liquids: Examples from Recent Measurements and a Critique of the So-Called Ideal KCl Line for the Walden Plot. *J. Chem. Eng. Data* **2010**, *55* (5), 1784–1788. https://doi.org/10.1021/je900878j.

(45) Walden, P. Über Organische Lösungs- Und Ionisierungsmittel: III. Teil: Innere Reibung Und Deren Zusammenhang Mit Dem Leitvermögen. *Z. Für Phys. Chem.* **1906**, *55U* (1), 207–249. https://doi.org/10.1515/zpch-1906-5511.

(46) Apelblat, A. Limiting Conductances of Electrolytes and the Walden Product in Mixed Solvents in a Phenomenological Approach. *J. Phys. Chem. B* **2008**, *112* (23), 7032–7044. https://doi.org/10.1021/jp802113v.

(47) Ue, M.; Mori, S. Mobility and Ionic Association of Lithium Salts in a Propylene Carbonate-Ethyl Methyl Carbonate Mixed Solvent. *J. Electrochem. Soc.* **1995**, *142* (8), 2577–2581. https://doi.org/10.1149/1.2050056.

(48) Webber, A. Conductivity and Viscosity of Solutions of LiCF3 SO 3, Li (CF 3 SO 2) 2 N , and Their Mixtures. *J. Electrochem. Soc.* **1991**, *138* (9), 2586–2590. https://doi.org/10.1149/1.2087287.

(49) Timachova, K.; Newman, J.; Balsara, N. P. Theoretical Interpretation of Ion Velocities in Concentrated Electrolytes Measured by Electrophoretic NMR. *J. Electrochem. Soc.* **2019, *166* (2), A264–A267. https://doi.org/10.1149/2.0591902jes.**

(50) John Newman; Nitash Balsara. *Electrochemical Systems*; John Wiley & Sons Inc., 2021.

(51) Pesko, D. M.; Feng, Z.; Sawhney, S.; Newman, J.; Srinivasan, V.; Balsara, N. P. Comparing Cycling Characteristics of Symmetric Lithium-Polymer-Lithium Cells with Theoretical Predictions. *J. Electrochem. Soc.* **2018**, *165* (13), A3186–A3194. https://doi.org/10.1149/2.0921813jes.

(52) Frenck, L.; Veeraraghavan, V. D.; Maslyn, J. A.; Balsara, N. P. Comparing Measurement of Limiting Current in Block Copolymer Electrolytes as a Function of Salt Concentration with Theoretical Predictions. *Electrochimica Acta* **2022**, *409*, 139911. https://doi.org/10.1016/j.electacta.2022.139911.

(53) Shah, D. B.; Kim, H. K.; Nguyen, H. Q.; Srinivasan, V.; Balsara, N. P. Comparing Measurements of Limiting Current of Electrolytes with Theoretical Predictions up to the Solubility Limit. *J. Phys. Chem. C* **2019**, *123* (39), 23872–23881. https://doi.org/10.1021/acs.jpcc.9b07121.

(54) Stolz, L.; Hochstädt, S.; Röser, S.; Hansen, M. R.; Winter, M.; Kasnatscheew, J. Single-Ion *versus* Dual-Ion Conducting Electrolytes: The Relevance of Concentration Polarization in Solid-State Batteries. *ACS Appl. Mater. Interfaces* **2022**, *14* (9), 11559–11566. https://doi.org/10.1021/acsami.2c00084.

(55) Mistry, A.; Yu, Z.; Peters, B. L.; Fang, C.; Wang, R.; Curtiss, L. A.; Balsara, N. P.; Cheng, L.; Srinivasan, V. Toward Bottom-Up Understanding of Transport in Concentrated Battery Electrolytes. *ACS Cent. Sci.* **2022**, *8* (7), 880–890. https://doi.org/10.1021/acscentsci.2c00348.

(56) Mistry, A.; Srinivasan, V.; Steinrück, H. Characterizing Ion Transport in Electrolytes via Concentration and Velocity Profiles. *Adv. Energy Mater.* **2023**, *13* (9), 2203690. https://doi.org/10.1002/aenm.202203690.

(57) Klett, M.; Giesecke, M.; Nyman, A.; Hallberg, F.; Lindström, R. W.; Lindbergh, G.; Furó, I. Quantifying Mass Transport during Polarization in a Li Ion Battery Electrolyte by in Situ ^{7} Li NMR Imaging. *J. Am. Chem. Soc.* **2012**, *134* (36), 14654–14657. https://doi.org/10.1021/ja305461j.

(58) Gribble, D. A.; Frenck, L.; Shah, D. B.; Maslyn, J. A.; Loo, W. S.; Mongcopa, K. I. S.; Pesko, D. M.; Balsara, N. P. Comparing Experimental Measurements of Limiting Current in Polymer Electrolytes with Theoretical Predictions. *J. Electrochem. Soc.* **2019**, *166* (14), A3228–A3234. https://doi.org/10.1149/2.0391914jes.

(59) Diederichsen, K. M.; McShane, E. J.; McCloskey, B. D. Promising Routes to a High Li^{+} Transference Number Electrolyte for Lithium Ion Batteries. *ACS Energy Lett.* **2017**, *2* (11), 2563–2575. https://doi.org/10.1021/acsenergylett.7b00792.

(60) Ueno, K.; Yoshida, K.; Tsuchiya, M.; Tachikawa, N.; Dokko, K.; Watanabe, M. Glyme–Lithium Salt Equimolar Molten Mixtures: Concentrated Solutions or Solvate Ionic Liquids? *J. Phys. Chem. B* **2012**, *116* (36), 11323–11331. https://doi.org/10.1021/jp307378j.

(61) Zhang, C.; Ueno, K.; Yamazaki, A.; Yoshida, K.; Moon, H.; Mandai, T.; Umebayashi, Y.; Dokko, K.; Watanabe, M. Chelate Effects in Glyme/Lithium Bis(Trifluoromethanesulfonyl)Amide Solvate Ionic Liquids. I. Stability of Solvate Cations and Correlation with Electrolyte Properties. *J. Phys. Chem. B* **2014**, *118* (19), 5144–5153. https://doi.org/10.1021/jp501319e.

(62) Schmidt, F.; Schönhoff, M. Solvate Cation Migration and Ion Correlations in Solvate Ionic Liquids. *J. Phys. Chem. B* **2020**, *124* (7), 1245–1252. https://doi.org/10.1021/acs.jpcb.9b11330.

(63) Mynam, M.; Kumari, S.; Ravikumar, B.; Rai, B. Effect of Temperature on Concentrated Electrolytes for Advanced Lithium Ion Batteries. *J. Chem. Phys.* **2021**, *154* (21), 214503. https://doi.org/10.1063/5.0049259.

(64) Lundgren, H.; Behm, M.; Lindbergh, G. Electrochemical Characterization and Temperature Dependency of Mass-Transport Properties of $LiPF_6$ in EC:DEC. *J. Electrochem. Soc.* **2015**, *162* (3), A413–A420. https://doi.org/10.1149/2.0641503jes.

(65) Gering, Kevin L.; Tien Q. Duong. Prediction of Electrolyte Transport Properties Using a Solvation-Based Chemical Physics Model., 2003.
(66) Hall, D. S.; Self, J.; Dahn, J. R. Dielectric Constants for Quantum Chemistry and Li-Ion Batteries: Solvent Blends of Ethylene Carbonate and Ethyl Methyl Carbonate. *J. Phys. Chem. C* **2015**, *119* (39), 22322–22330. https://doi.org/10.1021/acs.jpcc.5b06022.
(67) Fang, C.; Halat, D. M.; Balsara, N. P.; Wang, R. Dynamic Heterogeneity of Solvent Motion and Ion Transport in Concentrated Electrolytes. *J. Phys. Chem. B* **2023**, *127* (8), 1803–1810. https://doi.org/10.1021/acs.jpcb.2c08029.

Symbol List

t_{+}^{0}	Cation transference number with respect to the solvent velocity
κ	Ionic conductivity (S cm^{-1})
D	Salt diffusion coefficient (cm^2 s^{-1})
T_f	Thermodynamic factor
ρ_{+}	Current fraction
r	Measure of ratio of lithium ions to oxygen atoms in solvent
ρ	Density
η	Viscosity
R_s	Series resistance (Ω)
τ	Tortuosity of separator
φ_c	Volume fraction of conducting phase in separator
l	Thickness of the separator (cm)
A	Area of electrodes (cm^2)
$R_{i,0}$	Initial interfacial resistance (Ω)
$R_{i,ss}$	Steady state interfacial resistance (Ω)
I_{ss}	Steady state current (mA)
I_Ω	Initial current calculated via Ohm's law, $I_\Omega = \Delta V / R_T$ (mA)
U	Open circuit potential (mV)
k_0	Offset voltage (mV)
a	Fit parameter for restricted diffusion
b	Fit parameter for restricted diffusion
t	Time (s)
D_s	Salt diffusion coefficient through the separator (cm^2 s^{-1})
α	Minimum time cutoff for restricted diffusion
U	Open circuit potential, measured in concentration cells
m	Molality (mol kg^{-1})
r_{max}	Salt concentration with maximum conductivity
κ_{max}	Value of conductivity at r_{max}
Λ	Molar conductivity
v_{+}	Cation velocity (μm cm^{-1})
v_{-}	Anion velocity (μm cm^{-1})
v_0	Solvent velocity (μm cm^{-1})
$\gamma_{\pm}$	Mean molar activity coefficient
F	Faraday's constant (C mol^{-1})

R	Universal gas constant (8.314 J mol^{-1} K^{-1})
T	Temperature (°C)
D	Stefan-Maxwell diffusion coefficient (cm^2 s^{-1})
c	Concentration of the salt (mol cm^{-3})
c_0	Concentration of the solvent (mol cm^{-3})
c_T	Total concentration of the salt and solvent, $c_T = c_0 + c$ (mol cm^{-3})
i_{ss}	Steady-state applied current density, used in concentration gradient modeling (mA cm^{-2})
L	Distance between electrodes, used in concentration gradient modeling
$z_{-¿¿}$	Anion charge number
$v_{-¿¿}$	Number of anions the salt dissolves into
x/L	Dimensionless position across the electrolyte, used in concentration gradient modeling
Φ_{ss}	Steady-state potential from concentration gradient modeling (V)
r_{avg}	Average concentration of the electrolyte, used in concentration gradient modeling